



Shear stiffening in the microbuckling of fiber composites

Guillaume De Luca *

University of Colorado, Boulder, Colorado, 80309, USA

Francisco López Jiménez†

University of Colorado, Boulder, Colorado, 80309, USA

Thin composite laminates show higher flexural strength than expected based on their tensile and compressive properties. We analyze how shear stiffening, due to different buckling amplitudes along the thickness, result in delayed compressive failure. We use an analytical model to homogenize the energy of the laminate during microbuckling, and we use energy minimization to determine the onset-of-instability. We explore to different loading cases, constrained compression and bending, and we compare them to the case of an infinite laminate under pure compression. Our model predicts a significant increase in buckling load due to in-plane shear. The results also show clear thickness dependence, with a much higher predicted buckling load for thin samples.

I. Introduction

High strain composites are a class composite materials designed to operate at strains higher than 1% in bending [1]. This makes them very useful in the design of deployable space structures that rely on elastic deformation of structural elements during stowage, such as booms [2–4], antennas [5], and hinges for telescopes [6]. They often consist of very thin laminates of carbon fiber reinforced epoxy, and their bending failure properties are fundamentally different from those of thick composites, such that traditional failure models significantly underpredict their failure curvature. A series of recent studies have focused on developing the Column Bending Test as a standardized experimental procedure to characterize the bending failure properties of high strain composites at large curvatures [7–9]. However, the specific micromechanics of thin laminates are not well understood, and reliable predictive tools have not been developed yet. As a result, designs rely on experimental data that is hard to extend to fibers and laminate architectures.

Figure 1 shows experimental results on the failure of IM7 unidirectional carbon fibers, with a fiber volume fraction of approximately $V_f = 51\%$ and different thicknesses. They have been obtained using the Column Bending Test, and the results show the nominal bending strain at failure as a function of the laminate thickness. The results highlight three of the main differences with respect to traditional composites. First, there is a very clear dependence on the thickness, with the failure strain increasing as the thickness decreases. Second, the nominal strain at failure for specimens with $t < 500 \mu\text{m}$ are higher than the ultimate elongation at failure reported by the manufacturer, $\epsilon = 1.6\% - 1.9\%$. Finally, the samples failed in tension, see Figure 1(e), while bending of composites usually results in microbuckling failure on the compression side [10, 11]. The development of a failure criteria for high strain composites requires explaining the micromechanics leading to these differences.

The current hypothesis requires the combination of several factors that, while not important for thick laminates, have a big influence in the case of thin composites. First, the tensile stress is localized in very small regions, due to the small gauge length and the shift in neutral axis caused by the nonlinearity of the fibers. This, combined with the probabilistic nature of carbon fiber failure [12], explains why the tension side can sustain strains higher than the value expected from tensile tests. Second, microbuckling failure in compression is inhibited due to a phenomena called shear stabilization [7, 13]: in thin specimens the fibers in the compression and tension sides are very close to each other. In order to buckle, the fibers will need to significantly shear the matrix between them and the fibers in tension, which increases the load necessary for the onset-of-instability, in practice stabilizing the compressed fibers.

Figure 2 presents an schematic of the scenario, including the tensile and compression failure curves, as well as the failure envelope. Thick laminates fail in compression, at a roughly constant strain, while thin laminates, such as those in

*Visiting Student, Ann and H.J. Smead Department of Aerospace Engineering Sciences, University of Colorado, Boulder

†Assistant Professor, Ann and H.J. Smead Department of Aerospace Engineering Sciences, University of Colorado, Boulder, AIAA Member.

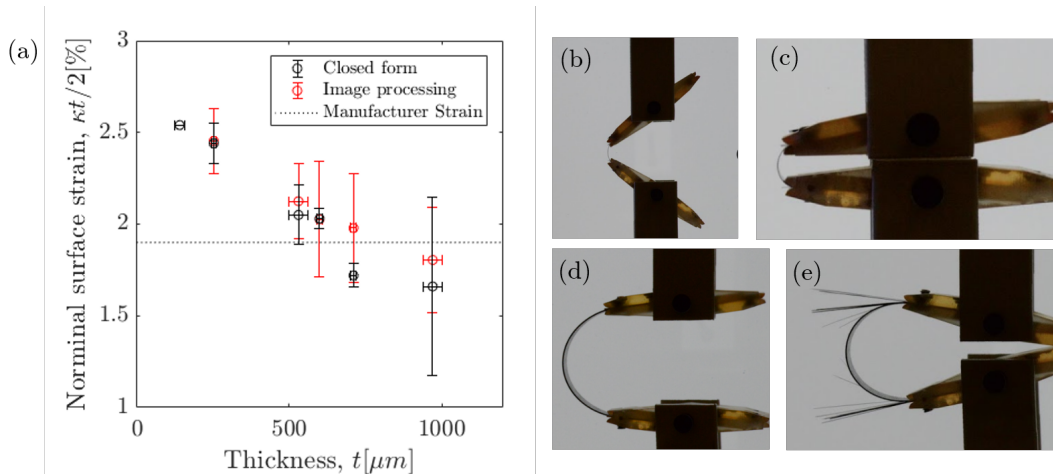


Fig. 1 Experimental results on unidirectional IM7 laminates. (a) Nominal strain at failure as a function of laminate thickness. The curvatures were assessed using a geometrical closed form approximate solution, as well as image processing of test images. (b-c) The thinnest samples, with $t \approx 141 \mu\text{m}$, did not break; the reported curvature represents the maximum curvature applied during the test. (d-e) The rest of samples failed in tension.

Figure 1(a), fail in tension. This requires a given thickness in which the most critical mechanism shifts, and which would in fact provide a mechanics-based criteria to determine what constitutes a thin laminate, at least for the purpose of bending failure. The goal of this paper is to provide insight on the micromechanics leading to shear stiffening. This will be done through homogenization-based micromechanical modeling. We consider the case of bending, which inspired the research, as well as compression in which buckling is artificially constrained in one the surfaces of the laminate, in order to create the conditions leading to shear between fibers with different buckling amplitude.

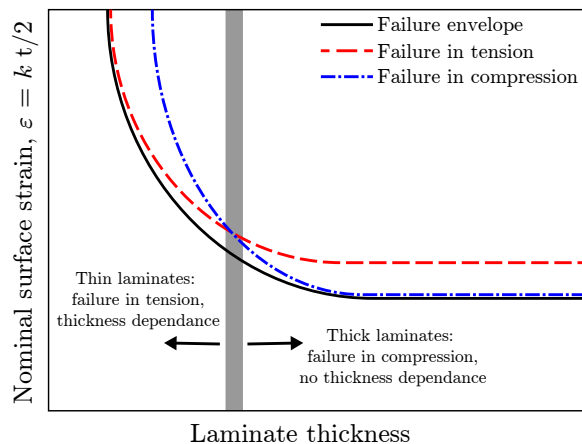


Fig. 2 Schematic of the hypothesized failure mechanisms in the bending of high strain composites, showing two different regimes: thin laminates, in which tension is the dominant failure mechanisms, and thick laminates, which fail in compression.

II. Analytical modeling

The modeling of microbuckling often follows the pioneering work of Rosen [14], considering the energy of fibers and matrix independently, and determining the onset of instability through energy minimization. In our case, the main difference with studies of microbuckling under pure compression is that the buckling amplitude is not constant through the specimen [15–18]. The shearing of the matrix between fibers with different buckling amplitude is the main physical

phenomena behind shear stabilization, and as such it is important to model the behavior of the composite through the thickness. A similar approach was followed by the authors in a previous work developed in a large deformation setting [19].

We consider a laminate with unidirectional fibers, parallel to the X_1 direction, with infinite width extending in the X_2 and finite thickness t extending in the X_3 direction. The fibers are assumed to be perfectly parallel cylinders of radius r , and the volume fraction is V_f . The boundary conditions are such that one at the face $X_3 = 0$ all displacement in the X_2 and X_3 is constrained.

The matrix is assumed to be isotropic, with Young's modulus E_m and Poisson's ratio ν_m . The fibers are transversely isotropic, with properties given by the stiffnesses E_{f1} , $E_{f2} = E_{f3}$, shear moduli $G_{f12} = G_{f13}$ and G_{f23} , and Poisson's ratios $\nu_{f12} = \nu_{f13}$ and ν_{f23} .

The laminate experiences an applied strain $\varepsilon_a(X_3)$ in the fiber direction, which can potentially vary through the thickness, in order to model combinations of bending and pure compression. At any given point this strain can result in pure compression of the laminate, ε_c , or equivalent shortening due to the microbuckling, ε_b , with:

$$\varepsilon_a(X_3) = \varepsilon_c(X_3) + \varepsilon_b(X_3), \quad (1)$$

which implies that we do not assume that fibers go into pure bending once they buckle. The buckled fibers are assumed to follow a sine wave, constrained in the $X_1 - X_2$ plane, with profile:

$$v = a(X_3) \sin \frac{\pi X_1}{\lambda}, \quad (2)$$

where the wavelength λ is assumed to be the same for all buckled fibers in the laminate. The strain due to bending, ε_b , is the result of the difference between the wavelength, λ , and the arc-length of the buckle, L_b :

$$\varepsilon_b = \frac{\lambda - L_b}{L_b}, \quad (3)$$

where L_b is calculated as:

$$L_b = \int_0^\lambda \sqrt{1 + \left(\frac{a^2 \pi^2}{\lambda^2} \sin \frac{\pi x}{\lambda} \right)^2} dx. \quad (4)$$

Once the geometry of the buckled fibers is defined, it is possible to calculate the strain energy of each component of the composite. The strain energy density of the laminate, W , is calculated as the sum of the energy of the matrix and the fibers:

$$W = W_m + W_f. \quad (5)$$

The strain of the fibers will be the sum of the energy due to pure compression of the fibers, and the energy due to microbuckling:

$$W_f = W_{f,c} + W_{f,b}. \quad (6)$$

The compression component can be calculated from ε_c as an integral along the thickness, due to the fact that the strain is not necessarily constant:

$$W_{f,c} = \frac{V_f}{t} \int_0^t \frac{1}{2} E_{f1} \varepsilon_c^2(X_3) dX_3. \quad (7)$$

The bending component is calculated from the buckled shape of the fibers. We assume that, due to the small displacements, the curvature of the buckled beam can be approximated as:

$$\kappa(X_1, X_3) = \frac{\partial^2 v(X_1, X_3)}{\partial X_3^2} = -\frac{a(X_3) \pi^2}{\lambda^2} \sin \frac{\pi X_1}{\lambda} . \quad (8)$$

The strain energy of a given fiber, integrated over the wavelength of the buckled geometry, is equal to:

$$W_{1f,b} = \int_0^\lambda \frac{1}{2} \kappa(X_1, X_3)^2 E_{1f} I dX_1 = \frac{a^2(X_3) \pi^4}{4\lambda^3} , \quad (9)$$

where I is the second moment of inertia of the fiber, $I = \pi r^4/4$.

The strain energy density due to the buckled fibers is obtained dividing by the volume of one fiber, and accounting for the fiber volume fraction:

$$W_{f,b} = V_f \frac{W_{1f,b}}{\pi r^2 \lambda} . \quad (10)$$

The energy density of the matrix can also be considered the sum of two terms: the energy due to the compression of the laminate, $W_{m,c}$, and the energy due to the buckled fibers, $W_{m,b}$, which corresponds to the shearing of the matrix. For the first term, we use an expression similar to Equation 7:

$$W_{m,c} = \frac{1 - V_f}{t} \int_0^t \frac{1}{2} E_m \varepsilon_c^2(X_3) dX_3 . \quad (11)$$

The energy due to the buckling of the fibers is due to two different shear terms:

$$W_{m,b} = W_{m,12} + W_{m,23} , \quad (12)$$

where $W_{m,12}$, due to shear in the $X_1 - X_2$ plane between fibers with the same buckling amplitude, is the term observed in buckling under pure compression, and $W_{m,23}$, due to shear in the $X_2 - X_3$ plane between fibers with different buckling amplitude, is the term that results in shear stiffening. The corresponding shear terms, for the homogenized composite (as opposed to local strains within the matrix at the microscopic scale) are given by:

$$\gamma_{12} = \frac{\partial v}{\partial X_1} = \frac{a \pi}{\lambda} \cos \frac{\pi X_1}{\lambda} , \quad (13)$$

$$\gamma_{23} = \frac{\partial v}{\partial X_3} = \frac{da}{dX_3} \sin \frac{\pi X_1}{\lambda} , \quad (14)$$

where the term da/dX_3 is calculated numerically.

The corresponding energy density terms are then:

$$W_{m,12} = \frac{1}{\lambda t} \int_0^t \int_0^\lambda \frac{1}{2} \hat{G}_{m,12} \gamma_{12}^2 dX_1 dX_3 = \int_0^t \frac{\hat{G}_{m,12} a^2 \pi^2}{4 \lambda^2 t} dX_3 , \quad (15)$$

$$W_{m,23} = \frac{1}{\lambda t} \int_0^t \int_0^\lambda \frac{1}{2} \hat{G}_{m,23} \gamma_{23}^2 dX_1 dX_3 = \int_0^t \frac{\hat{G}_{m,23}}{4t} \left(\frac{da}{dX_3} \right)^2 dX_3 , \quad (16)$$

where $\hat{G}_{m,ij}$ is the matrix contribution to the laminate shear stiffness G_{ij} , which takes into account not only the matrix properties, but also the properties of the fiber and the geometry at the microstructure level. In the limit of matrix and

fiber with the same properties, $G_m = G_f$, then $\hat{G}_{m,ij} = (1 - V_f) G_{ij}$, due to simple rule of mixtures. In the limit of a rigid fiber, where all the strain energy is on the fiber, then $G_{m,ij} = G_{ij}$.

The independent variables of the problem are the wavelength, λ , and the amount of applied strain that goes into pure compression at every point, $\varepsilon_c(X_3)$. The value of the variables is found through energy minimization, using the command `fminsearchbnd` in Matlab. The value of ε_c is discretized over a set of equispaced points along the thickness. The same discretization is used to define the profile of the applied loading, ε_d .

III. Results

A. Material properties

During our simulations, we use the properties of IM7 fibers and PMTF7, which were used to obtain the results in Fig. 1. The properties use for both components are listed in Table 1. The volume fraction is $V_f = 55\%$.

Matrix properties	
Young's modulus, E_m	3.496 GPa
Poisson's ratio, ν_m	0.37
Fiber properties	
Radius, r	2.6 μm
Axial stiffnes, E_{f1}	276 GPa
Tranverse stiffnes, $E_{f2} = E_{f3}$	13.8 GPa
Axial shear stiffness, $G_{f12} = G_{f13}$	9.5 GPa
Transverse shear stiffness, G_{f23}	5.52 GPa
Possion ratio, $\nu_{f12} = \nu_{f13}$	0.22
Possion ratio, ν_{f23}	0.25

Table 1 Fiber and matrix properties.

The properties of the laminate are obtained using the following set of equations [20]:

$$E_1 = E_{f1} V_f + E_m (1 - V_f) \quad (17)$$

$$\eta = \frac{\frac{E_{f2}}{E_m} - 1}{\frac{E_{f2}}{E_m} + 2} \quad (18)$$

$$E_2 = E_3 = E_m \frac{1 + 2\eta V_f}{1 - \eta V_f} \quad (19)$$

$$\nu_{12} = \nu_{13} = \nu_{f12} V_f + \nu_m (1 - V_f) \quad (20)$$

$$S_3 = 0.49247 - 0.47603 V_f - 0.02748 V_f^2 \quad (21)$$

$$G_{12} = G_m \frac{1 + V_f \left(1 - \frac{G_m}{G_{f12}}\right)}{\frac{G_m}{G_{f12}} + S_3 \left(1 - \frac{G_m}{G_{f12}}\right)} \quad (22)$$

$$\eta_4 = \frac{3 - 4\nu_m + \frac{G_m}{G_{f23}}}{4(1 - \nu_m)} \quad (23)$$

$$G_{23} = G_m \frac{V_f + \eta_4 (1 - V_f)}{\eta_4 (1 - V_f) + V_f \frac{G_m}{G_{f23}}} \quad (24)$$

We will assume that $\hat{G}_{m,ij} = (1 - V_f/2)G_{ij}$, which is the intermediate case between the two limits described in Section II. For clarity, compressive strain is presented as positive.

We will consider two different loading cases. The first one is compression in which microbuckling is artificially constrained on the layer with $X_3 = 0$, see Figure 3. This case does not correspond to any realistic scenario, but allows us to study the effect of shear stiffening when the laminate is under constant loading, and to decouple the relationship between thickness and applied strain. The second case corresponds to the more realistic case of bending of the laminate, in which the strain is a linear function of the distance to the neutral surface, assumed to be at the center.

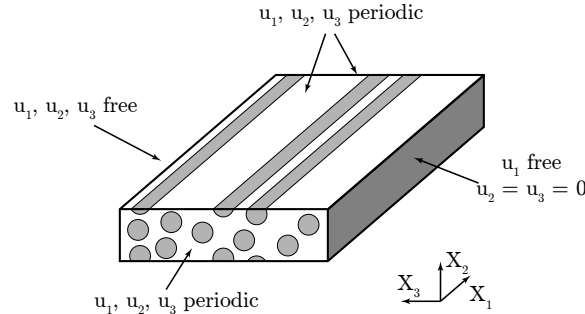


Fig. 3 Schematic of the model user for constrained compression, including boundary conditions on each face.

B. Constrained compression

Figure 4 shows the strain energy, as a function of the applied strain, of three possible cases: the linear response, with no buckling allowed; buckling with no constraints; and buckling when one face is constrained, resulting in shear stiffening, for increasing values of the thickness. The results clearly show that the constrain results in an increase of the strain necessary to cause an instability, with a clear thickness dependence.

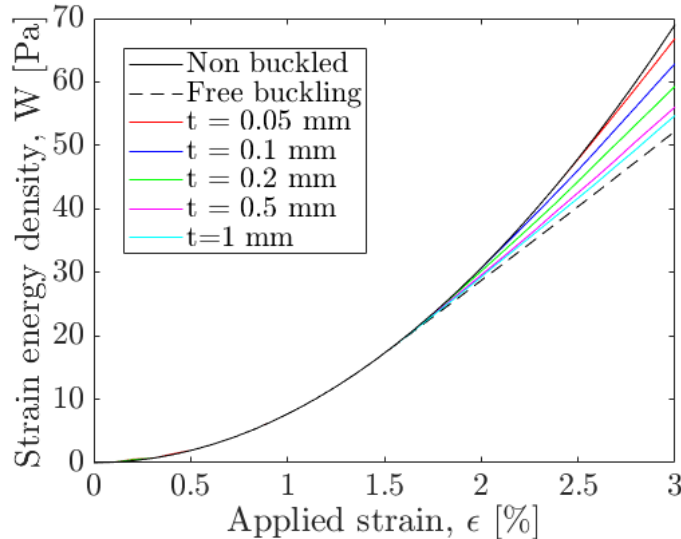


Fig. 4 Strained energy of different laminates under pure and constrained compression, as a function of the applied strain.

Figure 5 shows results from the same calculations, expressed as stress-strain, where the stress has been calculated as $\sigma = \frac{\partial W}{\partial \epsilon}$. The axis have been chosen to focus on the instability-onset. The data shows how shear stabilization result in an increase of close to 1% in the buckling applied strain. Even if models following the approach of Rosen [14] have

been shown to overestimate the buckling load, we believe that

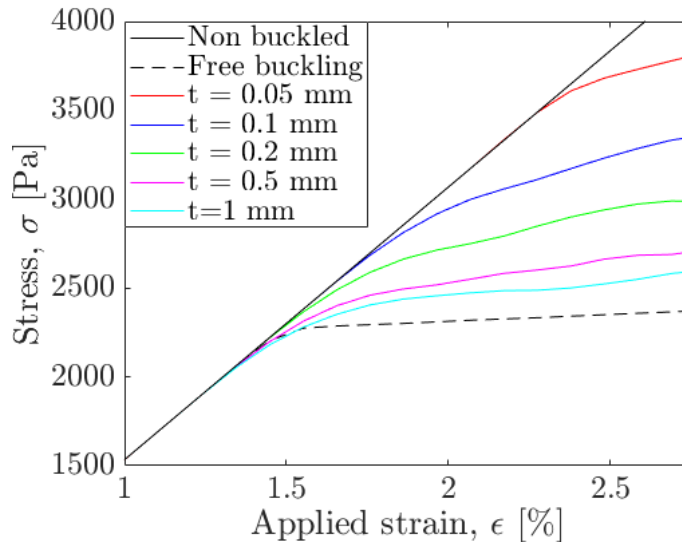


Fig. 5 Stress-strain relationship of different laminates under pure and constrained compression.

C. Bending

We now consider the case of bending. The applied strain varies now linearly across the arc-length, with a maximum applied strain at the out surface of $\varepsilon = \frac{2\kappa}{t}$, where κ is the curvature. The results have been normalized to eliminate the thickness dependence, so that different laminates can be compared. Figure 6 shows the results, as normalized bending moment (M/t) versus the strain at the surface of the laminate ($\varepsilon = \kappa t/2$). Again, we see a significant increase of the load necessary to cause microbuckling, even for laminates of moderate thickness. The vertical dashed line corresponds to our prediction for microbuckling under pure compression, with no constraints.

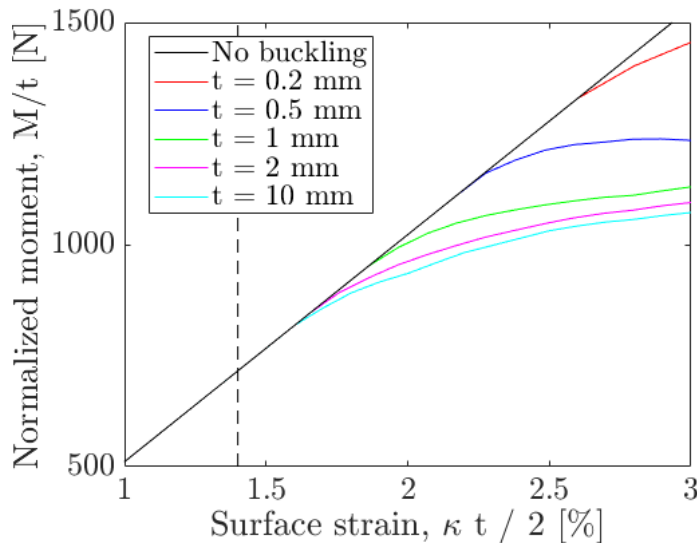


Fig. 6 Normalized moment versus surface strain, for different laminates under bending.

IV. Discussion and conclusions

We have presented a model for the microbuckling of thin buckling, which can apply different compression at different sections of the laminate, as well as directly inhibit buckling. This allows us to explore different conditions lead to shear stabilization, and compare it directly with buckling under pure compression. We have used it to explore the influence of the thickness for a given choice of laminate. Our results indicate that in-plane shear strain between layers with different buckling amplitude results in an increase in the load necessary to cause buckling, and that this increase is more pronounced for thin laminates.

We are currently working on developing finite element simulations at the micromechanics scale, which could be used to verify our model, not only at the macroscopic level (wavelength and buckling load), but also on local fields, such as maximum stress in either fiber or matrix. Experimental validation is also important. This could be achieved in the bending case, although since the specimens fail in tension before microbuckling takes place, complete validation in the thin range is complicated.

Several improvements and refinements could be incorporated, such as including fiber non-linearity, as well as initial imperfections and other geometries. Finally, it is important to highlight that this work should be combined with an analysis of the tensile failure of High Strain Composites, since it is the interplay between both phenomena what is going to determine the failure of the laminate, which is key prediction missing when considering the use of HSCs in industrial applications.

References

- [1] Murphey, T. W., Francis, W., Davis, B., and Mejia-Ariza, J. M., “High strain composites,” *2nd AIAA Spacecraft Structures Conference*, 2015, p. 0942.
- [2] Mallikarachchi, H., and Pellegrino, S., “Design of ultrathin composite self-deployable booms,” *Journal of Spacecraft and Rockets*, Vol. 51, No. 6, 2014, pp. 1811–1821.
- [3] Leclerc, C., and Pellegrino, S., “Ultra-Thin Composite Deployable Booms,” *Proceedings of IASS Annual Symposia*, Vol. 2017, International Association for Shell and Spatial Structures (IASS), 2017, pp. 1–9.
- [4] Davis, B., Turse, D., and Francis, W. H., “The Deployment of Large De-Orbit Sails Utilizing High Strain Composite Booms,” *AIAA Scitech 2019 Forum*, 2019, p. 1750.
- [5] Cox, K., Davis, B., VanHalle, R., and Francis, W. H., “Flight Build of a Furled High Strain Composite Antenna for CubeSats,” *2018 AIAA Spacecraft Structures Conference*, 2018, p. 1678.
- [6] Echter, M. A., Silver, M. J., D’Elia, E., Peterson, M., and Reid, B. M., “Recent Developments in Precision High Strain Composite Hinges for Deployable Space Telescopes,” *2018 AIAA Spacecraft Structures Conference*, 2018, p. 0939.
- [7] Rose, T., Sharma, A., Seamone, A., López Jiménez, F., and Murphey, T. W., “Carbon Unidirectional Composite Flexure Strength Dependence on Laminate Thickness,” *Proceedings of the American Society for Composites—Thirty-third Technical Conference*, 2018.
- [8] Fernandez, J. M., and Murphey, T. W., “A Simple Test Method for Large Deformation Bending of Thin High Strain Composite Flexures,” *2018 AIAA Spacecraft Structures Conference*, 2018, p. 0942.
- [9] Sharma, A. H., Rose, T., Seamone, A., Murphey, T. W., and López Jiménez, F., “Analysis of the Column Bending Test for Large Curvature Bending of High Strain Composites,” *AIAA Scitech 2019 Forum*, 2019, p. 1746.
- [10] Chen, F., Bazhenov, S., Hiltner, A., and Baer, E., “Flexural failure mechanisms in unidirectional glass fibre-reinforced thermoplastics,” *Composites*, Vol. 25, No. 1, 1994, pp. 11–20.
- [11] Marissen, R., and Brouwer, H., “The significance of fibre microbuckling for the flexural strength of a composite,” *Composites science and technology*, Vol. 59, No. 3, 1999, pp. 327–330.
- [12] López Jiménez, F., and Pellegrino, S., “Failure of carbon fibers at a crease in a fiber-reinforced silicone sheet,” *Journal of Applied Mechanics*, Vol. 80, No. 1, 2013.
- [13] Peterson, M. E., and Murphey, T. W., “Large deformation bending of thin composite tape spring laminates,” *54th AIAA/ASME/ASCE/AHS/ASC Structures, Structural Dynamics, and Materials Conference*, 2013, p. 1667.

- [14] Rosen, B., *Fiber Composite Materials*, Metals Park, Ohio, 1965.
- [15] Drapier, S., Grandidier, J.-C., and Potier-Ferry, M., "Towards a numerical model of the compressive strength for long fibre composites," *European Journal of Mechanics-A/Solids*, Vol. 18, No. 1, 1999, pp. 69–92.
- [16] Murphey, T., Meink, T., and Mikulas, M., "Some micromechanics considerations of the folding of rigidizable composite materials," *19th AIAA Applied Aerodynamics Conference*, 2001, p. 1418.
- [17] Francis, W., Lake, M., Schultz, M., Campbell, D., Dunn, M., and Qi, H. J., "Elastic memory composite microbuckling mechanics: closed-form model with empirical correlation," *48th AIAA/ASME/ASCE/AHS/ASC Structures, Structural Dynamics, and Materials Conference*, 2007, p. 2164.
- [18] López Jiménez, F., and Pellegrino, S., "Folding of fiber composites with a hyperelastic matrix," *International Journal of Solids and Structures*, Vol. 49, No. 3-4, 2012, pp. 395–407.
- [19] Brachthausen Balcells, S., and Lopez Jimenez, F., "Using Non-Linear Homogenization to Model Fiber Microbuckling in the Bending of Soft Composites," *AIAA Scitech 2019 Forum*, 2019, p. 2025.
- [20] Barbero, E. J., *Introduction to composite materials design*, CRC press, 2017.